Interplay among helical order, surface effects, and range of interacting layers in ultrathin films

F. Cinti,[1,2,*] A. Rettori,[2] and A. Cuccoli[2]
[1]*Department of Physics, University of Alberta, Edmonton, Alberta, Canada T6G 2J1*
[2]*Department of Physics and Astronomy and CNISM, University of Florence, 50019 Sesto Fiorentino (FI), Italy*
(Received 22 December 2009; revised manuscript received 25 February 2010; published 12 April 2010)

The properties of helical thin films have been thoroughly investigated by classical Monte Carlo simulations. The employed model assumes classical planar spins in a body-centered tetragonal lattice, where the helical arrangement along the film growth direction has been modeled by nearest-neighbor and next-nearest-neighbor competing interactions, the minimal requirement to get helical order. We obtain that, while the in-plane transition temperatures remain essentially unchanged with respect to the bulk ones, the helical or fan arrangement is stabilized at lower and lower temperatures when the film thickness, n, decreases; in the ordered phase, increasing the temperature, a softening of the helix pitch wave vector is also observed. Moreover, we show also that the simulation data around both transition temperatures lead us to exclude the presence of a first-order transition for all analyzed sizes. Finally, by comparing the results of the present work to those obtained for other models previously adopted in literature, we can get a deeper insight about the entwined role played by the number (range) of interlayer interactions and surface effects in noncollinear thin films.

DOI: 10.1103/PhysRevB.81.134415 PACS number(s): 75.10.Hk, 64.60.an, 64.60.De, 75.40.Cx

I. INTRODUCTION

Low-dimensional frustrated magnetic systems[1] still raise great interest both in consequence of theoretical aspects[2] and in view of possible technological applications.[3] Besides conventional collinear phase transitions, in many new materials, other nontrivial and unconventional forms of ordering have been observed.[4,5] A quantity of particular interest in this context is the spin chirality, an order parameter which turned out to be extremely relevant in many different materials[6–9] and in particular for XY helimagnets, as Ho, Tb, or Dy.[10] In this case, a new universality class was predicted because a $\mathbb{Z}_2 \times SO(2)$ symmetry is spontaneously broken in the ordered phase:[2] the usual $SO(2)$ symmetry being related to spin variables $\vec{S}_i$ and the $\mathbb{Z}_2$ symmetry to the spin chirality $\kappa_{ij} \propto [\vec{S}_i \times \vec{S}_j]^z$. For these rare-earth elements, ultrathin films, where the noncollinear modulation is comparable to the film's thickness, have been obtained.[11] The lack of translational invariance turns out to be decisive in order to observe a drastic change of the magnetic structures.[12] Recent experimental data on ultrathin Ho films[13] have been lately interpreted and discussed[14,15] on the basis of classical Monte Carlo (MC) simulations of a spin Hamiltonian which is believed to give a realistic modeling of bulk Ho. Such Hamiltonian[16] allows for competitive middle-range interactions by including six different exchange constants along the c crystallographic axis and gives a helix pitch wave vector Q_z such that $Q_z c' \simeq 30°$, where $c'=c/2$ is the distance between nearest-neighboring spin layers parallel to the ab crystallographic planes, henceforth denoted also as $x-y$ planes, while z will be taken parallel to c. For $n>16$, n being the number of spin layers in the film, a correct bulk limit is reached, while for lower n, the film properties are clearly affected by the strong competition among the helical pitch and the surface effects, which involve the majority of the spin layers. In the range $n=9-16$, i.e., comparable to the helical pitch, three different magnetic phases emerged, with the high-T, disordered, paramagnetic phase and the low-T, long-range ordered one separated by an intriguing, intermediate-T block phase, where outer ordered layers coexist with some inner disordered ones. Finally, for $n \leq 7$, the film collapses once and for all to a quasicollinear order.

The complex phase diagram unveiled by such MC simulations awakens a further intriguing question: to what extent the observed behavior may be considered a simple consequence of the competition between helical order and surface effects? For example, is it just a matter of having such a competition or does the range of interactions also play a relevant role? Indeed, when the range of the interactions is large enough, we have a greater number of planes which can be thought of as "surface planes," i.e., for which the number of interacting neighbors is significantly reduced with respect to the bulk layers; therefore, we expect that the larger the interaction range, the stronger should be the surface effects. But, at the same time, the same modulation of the magnetic order can be achieved with different number of interacting layers: notably, nearest and next-nearest layer competitive interactions are enough to get a helical structure with whatever pitch wave vector. Such observation gives us a possible way to solve the conundrum previously emerged as we have the possibility of varying the range of interactions without modifying the helical pitch, thus decoupling the two relevant length scales along the film growth direction and making accessible a range of n of the order of, or smaller than, the helical pitch, but still large enough that a substantial number of layers can behave as "bulk" layers. Differently to the previous papers, here we investigate by MC simulations the properties of the same system by making use of the simplest model Hamiltonian able to describe the onset of a helical magnetic order in Ho, i.e., we consider only two interlayer coupling constants as previously done in Ref. 11.

The paper is organized as follows. In Sec. II, the model Hamiltonian will be defined, and the MC techniques, and all the thermodynamic quantities relevant for this study, will be presented. In Sec. III, the results obtained for different thicknesses will be presented, both in the matter of the critical properties of the model and of the magnetic ordered struc-

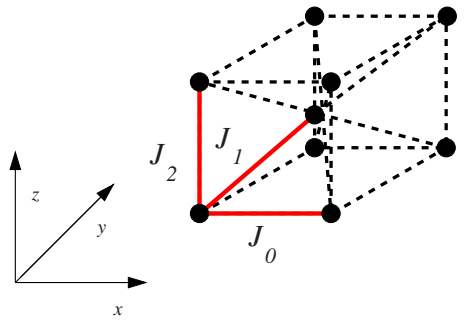

FIG. 1. (Color online) BCT lattice with J_0 in-plane coupling constant and out-of-plane J_1 and J_2 competing interactions.

tures observed. Finally, in Sec. IV, we shall discuss such results, drawing also some conclusions.

II. MODEL HAMILTONIAN AND MONTE CARLO OBSERVABLES

The model Hamiltonian we use in our simulations is the minimal one able to describe helimagnetic structures[1,17,18]

$$\mathcal{H} = -\left[J_0 \sum_{\langle ij \rangle} \vec{S}_i \cdot \vec{S}_j + J_1 \sum_{\langle ik \rangle} \vec{S}_i \cdot \vec{S}_k + J_2 \sum_{\langle il \rangle} \vec{S}_i \cdot \vec{S}_l \right], \quad (1)$$

where $\vec{S}_i$ are classical planar unit vectors representing the direction of the total angular momentum of the magnetic ions, whose magnitude $\sqrt{j(j+1)}$ ($j=8$ for Ho ions) is already encompassed within the definition of the interaction constants $J_{0,1,2}$. As sketched in Fig. 1, the magnetic ions are located on the sites of a body-centered tetragonal (BCT) lattice: the first sum appearing in the Hamiltonian describes the in-plane (xy) nearest-neighbor (NN) interaction, which is taken ferromagnetic (FM), with exchange strength $J_0>0$; the second sum represents the coupling, of exchange strength J_1, between spins belonging to NN planes along the z direction (which we will assume to coincide with the film growth direction); finally, the third sum takes into account the interaction, of exchange strength J_2, between spins lying on next-nearest-neighbor (NNN) planes along z. NN interaction J_1 can be taken both ferromagnetic or antiferromagnetic, but NNN coupling J_2 must be antiferromagnetic and the condition $|J_2|>|J_1|/4$ must be fulfilled. In the bulk limit, the ground-state energy per spin is equal to $e_g(Q_z) = \{-4J_0 - 2J_1[4\cos(Q_z c') + \delta \cos(2Q_z c')]\}$, where c' is the distance between NN layers, $\delta = \frac{J_2}{J_1}$, and $Q_z c' = \arccos(-\frac{1}{\delta})$ is the angle between spins lying on adjacent planes along the z direction. The helical arrangement in bulk Ho corresponds to $Q_z c' \simeq 30.5°$ (Ref. 10): such value can be obtained with the set of coupling constants $J_0=67.2$ K, $J_1=20.9$ K, and $J_2=-24.2$ K that we have employed in our simulations.

We will denote with n the film thickness, i.e., the number of spin layers along the z direction ($n=1-24$) and with $L\times L$ the number of spins in each layer (x and y directions, $L=8-64$). Periodic boundary conditions were applied along x and y, while free boundaries were obviously taken along z.

Thermal equilibrium was attained by the usual METROPOLIS algorithm,[19] supplemented by the overrelaxed technique[20] in order to speed-up the sampling of the spin-configuration space: a typical "MC step" was composed by four METROPOLIS and four to five overrelaxed moves per particle. Such judicious mix of moves is able both to get faster the thermal equilibrium and to minimize the correlation "time" between successive samples. For each T, we have usually performed three independent simulations, each one containing at least 2×10^5 measurements taken after discarding up to 5×10^4 Monte Carlo steps in order to assure thermal equilibration. In the proximity of the critical region, the multiple histogram (MH) technique was also employed[21] as it allows us to estimate the physical observables of interest over a whole temperature range in a substantially continuous way. For all the quantities of interest, the average value and the error estimate were obtained by the bootstrap resampling method[22] given that, as pointed out in Ref. 23, for a large-enough number of measurements, this method turns out to be more accurate than the usual blocking technique. In our implementation, we pick out randomly a sizable number of measurements (typically, between 1 and 1×10^4 for the single simulation and between 1 and 5×10^5 for the MH technique) and iterate the resampling at least 100 times.

The thermodynamic observables we have investigated include the FM order parameter for each plane l,

$$m_l = \sqrt{(m_l^x)^2 + (m_l^y)^2}, \quad (2)$$

which is related to the $SO(2)$ symmetry breaking. At the same time, turns out to be significant also is the average order parameter of the film, defined as

$$M = \frac{1}{n} \sum_{l=1}^{n} m_l. \quad (3)$$

Turning to the helical order, we can explore it along two different directions. The first one is by the introduction of the chirality order parameter[1,2]

$$\kappa = \frac{1}{4(n-1)L^2 \sin Q_z} \sum_{\langle ij \rangle} [S_i^x S_j^y - S_i^y S_j^x], \quad (4)$$

where the sum refers to spins belonging to NN layers, while Q_z is the bulk helical pitch vector. The second possibility[24] is that of looking at the integral

$$M_{\mathrm{HM}} = \frac{1}{K} \int_0^{\pi} dq_z S(\vec{q}), \quad (5)$$

where $S(\vec{q})$, with $\vec{q}=(0,0,q_z)$, is the structure factor along the z direction of the film, while the normalization factor K is the structure factor integral at $T=0$. Although the use of the last observable can be seen as a way to overcome the intrinsic difficulties met in defining a correct helical order parameter free of any undue external bias, we remind that such quantity has generally to be managed with particular care, as discussed in details in Refs. 14 and 15, where it was shown that the presence of block structures prevents us to unambiguously relate the evolution of $S(\vec{q})$ with the onset of helical order. However, for the specific case of the model under investigation, such quantity can still be considered a fairly

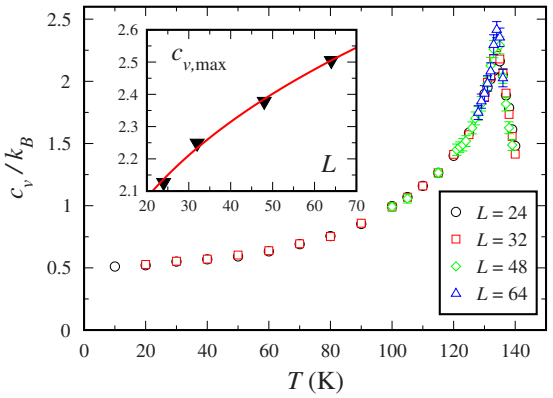

FIG. 2. (Color online) Specific heat c_v per spin vs temperature for thickness $n=16$ (for lateral dimension, see the legends). (Inset) Maximum of c_v vs L obtained through MH technique. The continuous red line is a power-law fit.

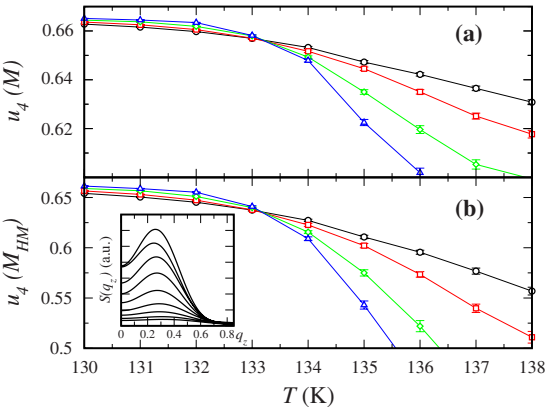

FIG. 3. (Color online) Binder cumulants at thickness $n=16$ (colors as in Fig. 2). (a) Binder cumulant for the order parameter defined in Eq. (3). (b) Binder cumulant extracted from the integral of the structure factor [see Eq. (5)]. (Inset) Structure factor for $L=64$ between $T=131$ K (upper curve) and $T=140$ K (lower) with 1 K temperature step.

significant order parameter as no block structures emerge from the simulations (see below).

In order to get a clear picture of the critical region and to give an accurate estimate of the critical temperature, we look also at the following quantities:

$$c_v = nL^2\beta^2(\langle e^2\rangle - \langle e\rangle^2), \tag{6}$$

$$\chi_o = nL^2\beta(\langle o^2\rangle - \langle o\rangle^2), \tag{7}$$

$$u_4(o) = 1 - \frac{\langle o^4\rangle}{3\langle o^2\rangle^2}, \tag{8}$$

where $\beta=1/k_BT$ and o is one of the relevant observables, i.e., $m_l, M, \kappa, M_{\mathrm{HM}}$. We present also the following symbols: by $T_N(n)$ we will denote the helical or fan phase-transition temperature for thickness n, $T_C(n)$ will instead indicate the ordering temperature of the sample as deduced by looking at the behavior of the average order parameter (3), while $T_C^l(n)$ will be the lth plane transition temperature related to the order parameter defined in Eq. (2).

III. RESULTS

The results obtained by our MC simulations will be presented starting from $n=16$ which still gives a bulklike behavior. In Fig. 2, the specific heat for $L=24$, 32, 48, 64 is shown. The location of the specific-heat maximum shows a quite definite evolution toward the bulk transition temperature, $T_N^{\mathrm{Ho}} \simeq 132$ K (Ref. 10) (for this model, the mean-field theory predicts $T_{N,\mathrm{MF}}^{\mathrm{Ho}} \simeq 198$ K). From finite-size scaling, a specific-heat critical exponent $\alpha=0.167(5)$ can be extrapolated: however, we remind that larger lattice sizes L are usually required to make the estimated values of the critical exponents well established.

The Binder cumulant[25] (8) for M close to the c_v peak temperature is shown in Fig. 3(a); its analysis leads to an estimate of $T_C(16)=133.2(5)$. The development of the helical arrangement of magnetization was investigated by looking at the integral of the structure factor $S(\vec{q})$ along the z direction and making again use of the cumulant analysis in order to locate the helical transition temperature at $T_N(16)=133.1(3)$ K [Fig. 3(b)]. The crossing points of the Binder's cumulants of the helical order parameter immediately appear to be located, within the error bars, at the same temperature of those for the average magnetization previously discussed. In addition, it is worthwhile to observe that the peak evolution of $S(0,0,q_z)$, in particular close to $T_N(16)$ [inset of Fig. 3(b)], displays the typical behavior expected for a helical structure. We can thus conclude that for $n=16$, as it is commonly observed in bulk samples, the establishment of the in-plane order coincides with the onset of the perpendicular helical arrangement at $T_N(16)$; however, due to helix distortion in the surface regions, the maximum of $S(0,0,q_z)$ stabilizes at values of q_z sensibly smaller [e.g., $Q_z[T_N(16)] \approx 16°$ and $Q_z(T=10\ \mathrm{K}) \approx 28°$] with respect to the bulk one ($Q_z^{\mathrm{Ho}}=30.5°$).

The MC simulation outcomes for $n=16$ we just presented appear quite different with respect to those obtained at the same thickness for the model with six coupling constants along the z direction.[14,15] Indeed, for the J_1-J_2 model here investigated, we observe that all layers order at the same temperature and we do not find any hint of the block phase with inner disordered planes intercalated to antiparallel *quasi*-FM four-layer blocks previously observed; sample MC runs we made using the same hcp lattice employed in Refs. 14 and 15 show that the presence or absence of the block phase is not related to the lattice geometry but it is a consequence of the interaction range only.

Now we describe and discuss MC simulation data for thinner samples. A synthesis of the results obtained for $n=8$ is shown in Figs. 4(a)–4(d). The specific heat c_v [Figs. 4(a)] reveals very small finite-size effects, which cannot be unambiguously detected for the largest lattice size ($L=64$), as they fall comfortably within the error range. The specific-heat maximum is located close to the bulk transition temperature as found for $n=16$ and the same is true for the crossing point of the Binder cumulant of M (not reported in figure), which is located at $T_C(8)=133.3(3)$ K. These data

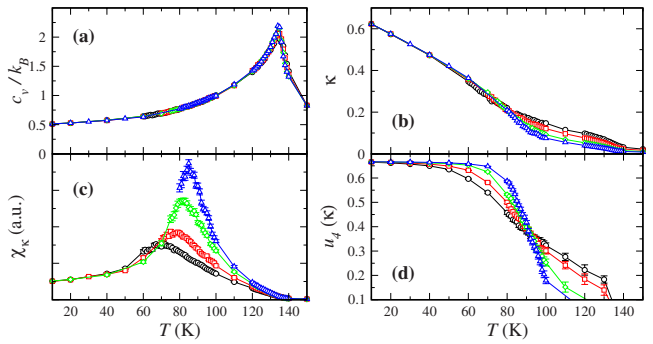

FIG. 4. (Color online) Thermodynamic quantities obtained for thickness $n=8$ in the temperature range of 0–150 K. Colors and symbols as in Fig. 2. (a) Specific heat. (b) Chirality order parameter. (c) Susceptibility χ_κ. (d) Binder cumulant for κ.

give a first indication that also for $n=8$ all the planes are still ordering almost at the same T; such property has been observed for all the investigated n below 16, so that $T_C(n)$ results quite n-independent (see also Fig. 5). Although the layer subtraction does not seem to modify $T_C(n)$, the onset of helical arrangement is observed to shift at lower temperatures as n decreases. The chirality κ is reported in Fig. 4(b) for $n=8$: around $T\sim 80$ K, we can identify a finite-size behavior of κ which, at variance with the previous one, can be easily recognized as typical of a phase transition. This is confirmed by the analysis of the chiral susceptibility χ_κ [Fig. 4(c)], which for the largest L has a maximum at $T=85$ K. Since the order parameter (4) is the relevant one to single out the onset of the fan arrangement, we can get a more accurate estimate of $T_N(8)$ by looking at the Binder cumulant $u_4(\kappa)$ [Fig. 4(d)]. By making use of the MH technique, we locate the crossing point at $T_N(8)=92(2)$ K. It is worthwhile to observe as the specific heat does not show any anomaly at $T_N(8)$ being the entropy substantially removed at $T_C(8)$.

The scenario just outlined for $n=8$ results to be correct in the thickness range $6\leq n\lesssim 15$, where a clear separation between $T_N(n)$ and $T_C(n)$ can be easily figured out. In such temperature window, the strong surface effects produce a *quasi*-FM setup of the magnetic film structure along the z direction. While leaving for the next section, a more detailed discussion of this regime, we report in Fig. 5 a plot of $T_N(n)$

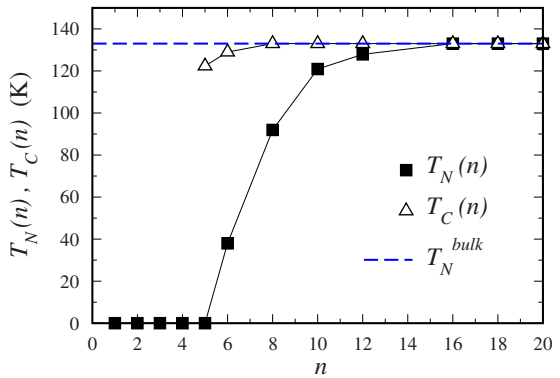

FIG. 5. (Color online) Transition temperatures $T_N(n)$ and $T_C(n)$ vs film thickness n.

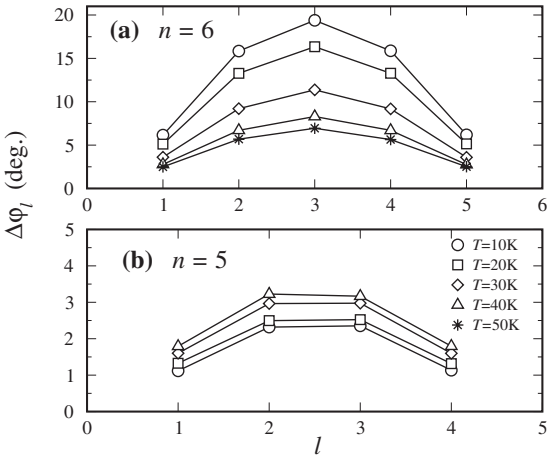

FIG. 6. Rotation angle $\Delta\varphi_l$ between magnetic moments on NN layers $(l+1,l)$ at some low temperatures, for thicknesses $n=5$ and $n=6$, and lateral dimension $L=64$.

and $T_C(n)$ for all the simulated thicknesses. The separation between the two critical temperatures is maximum for $n=6$, where $T_N(6)=38(4)$ K, that is, $T_N(6)\sim\frac{1}{3}T_C(6)$. For films with less than six layers, no fan order is observed, i.e., for $n=5$ and below, the chirality does not display any typical feature of fan ordering at any temperature below $T_C(n)$. As a representative quantity, we finally look at the rotation angle of the magnetization between nearest planes: $\Delta\varphi_l=\varphi_{l+1}-\varphi_l=\arccos[M_l^xM_{l+1}^x+M_l^yM_{l+1}^y]$, where (M_l^x,M_l^y) is the magnetization of each plane l. $\Delta\varphi_l$ is displayed in Figs. 6(a) and 6(b), for $n=6$ and $n=5$, respectively. In Fig. 6(a), a quite clear fan stabilization is observed when the temperature decreases, while in Fig. 6(b), i.e., for $n=5$, $\Delta\varphi_l$ keeps an almost temperature independent very small value. The absence of fan arrangement for $n\leq 5$ is simply due to the lack of "bulk planes" inside the film so that we are left with only a two-dimensional (2D) trend at $T_C(n)$.

IV. DISCUSSION AND CONCLUSION

A possible framework to analyze the results presented in the previous section is suggested by Fig. 5, where we can easily distinguish three significant regions: (i) high thickness, $n\geq 16$, where the films substantially display a bulk behavior, with the single planes ordering temperature coinciding with the helical phase-transition one; (ii) intermediate thickness, $6\leq n\lesssim 15$, where the temperature corresponding to the onset of in-plane order, $T_C(n)$, is still $\simeq T_N^{bulk}$, but where the helical or fan arrangement stabilizes only below a finite temperature $T_N(n)<T_C(n)$; (iii) low thickness, $1\leq n\leq 5$, where $T_C(n)\lesssim T_N^{bulk}$ but no fan phase is present at any temperature. The behavior in region (iii) can be attributed to the decreasing relevance of the contribution to the total energy of the system coming from the interactions among NNN planes as n decreases; moreover, the thinness of the film leads to an effective 2D-like trend. Region (ii) looks however more intriguing and requires a more accurate discussion, which can benefit from a careful comparison of the behavior of a given quantity in regions (i) and (ii).

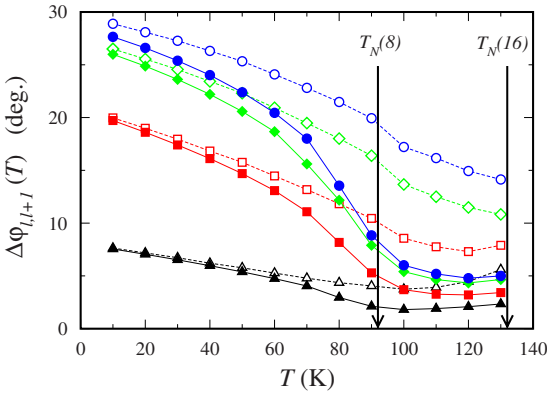

FIG. 7. (Color online) $\Delta\varphi_l(T)$ vs temperature for the surface planes $l=1$ (triangles), $l=2$ (squares), $l=3$ (diamonds), and $l=4$ (circles). Straight lines and full symbols: $n=8$. Dashed lines and open symbols: $n=16$.

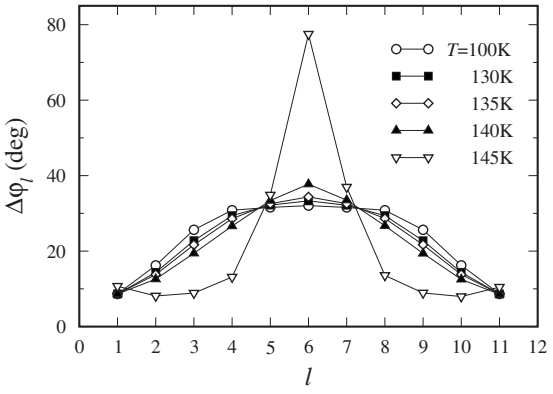

FIG. 8. $\Delta\varphi_l$ for a BCT lattice and $n=12$ when the six coupling constants set employed in Refs. 14 and 15 (see text) is used. The temperature range has been chosen around $T_C(n)$ (error bars lie within point size).

For this purpose, we look at the T dependence of the rotation angle of the magnetization between NN planes. In Fig. 7, $\Delta\varphi_l(T)$ for $n=8$ and $n=16$ is plotted for the outermost planes, $l=1\ldots4$. For both thicknesses, a monotonic trend is observed, but at variance with what happens for the highest thickness, for $n=8$ we see, starting from a temperature $T\lesssim T_N(8)$, an abrupt drop of $\Delta\varphi_3$ and $\Delta\varphi_4$, which rapidly reach an almost constant value only slightly larger than $\Delta\varphi_1$. In the range $T_N(8)\lesssim T<T_C(8)$, we thus substantially observe the same small phase shifts between all NN layers, testifying a stable quasi-FM configuration giving no contribution to the helical order parameters.

The absence of the block phase in the J_1-J_2 model has to be attributed to the different range of interactions, rather than to the different lattice structure, as we verified by performing some simulations using the same set of interaction constants employed in Refs. 14 and 15 but using a BCT lattice. The results we obtained for $\Delta\varphi_l$ with $n=12$ are reported in Fig. 8. The latter is absolutely similar to Fig. 7 of Ref. 15 and clearly displays the footmarks of the block phase (see down triangle), with two external blocks of ordered layers ($l=1\ldots5$ and $8\ldots12$), where $\Delta\varphi_l$ is roughly 10°, separated by a block of disordered layers and with almost opposite magnetization. We can thus confidently assert that, regardless of the underlying lattice structure, by decreasing the number of the out-of-plane interactions, for n close to the helical bulk pitch, the block phase is replaced by a quasi-FM configuration in the $T_N(n)<T<T_C(n)$.

Concerning the problem of the order of the transitions observed at $T_N(n)$ and $T_C(n)$, we focus our attention to the equilibrium probability distribution of the energy. For both temperatures and all investigated film thicknesses, no double-peak structure is observed, so that we have no direct indication for a first-order transition even if, according to precedent studies of Diep[17] and Loison,[18] the presence of a first-order transition at $T_N(n)$ cannot be completely excluded, as it could reveal itself only when the lateral dimension L is much larger than the largest correlation length. These findings agree with the results we got in previous MC simulations discussed in Ref. 15, so that we may conclude that the order of the observed transitions is not affected by the range of interactions.

In conclusion, our MC investigation has clearly shown that for the rare-earth ultrathin films, the phase diagram is strongly dependent on the chosen model. In particular, we would like to emphasize that the results presented prove that the intermediate block phase[14,15]—obtained by applying the six out-of-plane coupling-constant models as experimentally established for the bulk Ho (Ref. 16)—is absent when a simple two coupling constants model is assumed. Consequently, using experimental techniques able to probe local spin arrangements, such as slow muons relaxation,[26] could be helpful to check for the presence of a block phase, thus allowing us to discriminate between different models.

ACKNOWLEDGMENTS

This work was supported in part by the Natural Science and Engineering Research Council of Canada under Research Grant 121210893, and by the Alberta Informatics Circle of Research Excellence (iCore).

*cinti@ualberta.ca

[1] *Frustrated Spin Systems*, edited by H. T. Diep (World Scientific, Singapore, 2004).
[2] H. Kawamura, J. Phys.: Condens. Matter **10**, 4707 (1998).
[3] T. Kimura, T. Goto, H. Shintani, K. Ishizaka, T. Arima, and Y. Tokura, Nature (London) **426**, 55 (2003).
[4] F. Cinti *et al.*, Phys. Rev. Lett. **100**, 057203 (2008).
[5] J. H. Park, S. Onoda, N. Nagaosa, and J. H. Han, Phys. Rev. Lett. **101**, 167202 (2008), and references therein.
[6] S. W. Cheong and M. Mostovoy, Nature Mater. **6**, 13 (2007).
[7] M. Lee, W. Kang, Y. Onose, Y. Tokura, and N. P. Ong, Phys. Rev. Lett. **102**, 186601 (2009).

[8] P. Pedrazzini *et al.*, Phys. Rev. Lett. **98**, 047204 (2007).
[9] H. Kawamura and M. S. Li, Phys. Rev. Lett. **87**, 187204 (2001).
[10] P. J. Jensen and A. R. Mackintosh, *Rare Earth Magnetism (Structure and Excitations)* (Clarendon Press, Oxford, 1991).
[11] S. Konings, C. Schuessler-Langeheine, H. Ott, E. Weschke, E. Schierle, and J. Goedkoop, arXiv:0707.2765 (unpublished).
[12] P. J. Jensen and K. H. Bennemann, Surf. Sci. Rep. **61**, 129 (2006).
[13] E. Weschke *et al.*, Phys. Rev. Lett. **93**, 157204 (2004).
[14] F. Cinti, A. Cuccoli, and A. Rettori, Phys. Rev. B **78**, 020402(R) (2008).
[15] F. Cinti, A. Cuccoli, and A. Rettori, Phys. Rev. B **79**, 134420 (2009).
[16] J. Bohr, D. Gibbs, J. D. Axe, D. E. Moncton, K. L. D'Amico, C. F. Majkrzak, J. Kwo, M. Hong, C. L. Chien, and J. Jensen, Physica B **159**, 93 (1989).
[17] H. T. Diep, Phys. Rev. B **39**, 397 (1989).
[18] D. Loison, Physica A **275**, 207 (2000).
[19] N. Metropolis, A. W. Rosenbluth, M. N. Rosenbluth, A. H. Teller, and E. Teller, J. Chem. Phys. **21**, 1087 (1953).
[20] F. R. Brown and T. J. Woch, Phys. Rev. Lett. **58**, 2394 (1987).
[21] D. P. Landau and K. Binder, *A Guide to Monte Carlo Simulation in Statistical Physics* (Cambridge University Press, Cambridge, England, 2000).
[22] M. E. J. Newman and G. T. Barkema, *Monte Carlo Methods in Statistical Physics* (Clarendon Press, Oxford, 1999).
[23] B. Efron, Ann. Stat. **7**, 1 (1979).
[24] P. M. Chaikin and T. C. Lubensky, *Principles of Condensed Matter Physics* (Cambridge University Press, New York, 1995).
[25] K. Binder, Z. Phys. B **43**, 119 (1981); Phys. Rev. Lett. **47**, 693 (1981).
[26] T. J. Jackson, T. M. Riseman, E. M. Forgan, H. Glückler, T. Prokscha, E. Morenzoni, M. Pleines, Ch. Niedermayer, G. Schatz, H. Luetkens, and J. Litterst, Phys. Rev. Lett. **84**, 4958 (2000).